

Original Research

High Antimony Source and Geochemical Behaviors in Mine Drainage Water in China's Largest Antimony Mine

Cheng Li^{1,2}, Chunming Hao^{3,4,2*}, Wei Zhang³, Herong Gui⁴

¹Xi'an University of Science and Technology, Shaanxi, P.R. China

²Key Laboratory of Mine Geological Hazards Mechanism and Control, Shaanxi, P.R. China

³North China Institute of Science and Technology, Hebei, P.R. China

⁴National Engineering Research Center of Coal Mine Water Hazard Control, Suzhou University, Anhui, P.R. China

Received: 7 October 2019

Accepted: 1 December 2019

Abstract

The Sb source and the formation process of high Sb-contaminated mine water have not been well investigated. In this study, 11 mine water samples, 2 rainwater samples, 4 surface water samples, 4 D₃x⁴ (MA) water samples, and 4 D₃s⁴ (SA) water samples were collected from the largest antimony mine in China. The $\delta^{34}\text{S}$, $\delta^{18}\text{O}$, and $\delta^2\text{H}$ data and the water-rock interactions were analyzed to reveal the source of Sb and geochemical behaviors of the mine drainage water. The Sb concentrations in mine water samples are 238-2420 times higher than the maximum acceptable Sb concentration (0.005 mg/L), according to China's national drinking water quality standards. The chemical composition of the mine water is Ca-Na-SO₄, and the SA water is the main source of the mine water. It is also revealed that the Sb pollutant in the mine water is derived from the oxidation of stibnite. Moreover, the soluble oxygen in the mine water and the ion-exchange interaction between the mine water and surrounding rocks also contribute to the formation of high Sb-contaminated mine water. This study provides valuable information for Sb pollutant source control and water body protection in a mine area.

Keywords: antimony pollution, water-rock interaction, stable isotopes analysis, mine drainage water, geochemical source

Introduction

Antimony (Sb) is a versatile metal element and has found applications in flame retardants, batteries, solar cells, and semiconductor industries. The increasingly widespread usage of Sb has caused environmental

pollution. Recently, Sb has been detected in soil, water, river sediment, plants, and groundwater – especially in areas around Sb mines [1]. The Xikuangshan Mine in Hunan, China, known as the world's antimony capital [2], currently accounts for 90% of the world's total antimony ore production [3]. Numerous studies have been carried out in this area to evaluate the multimedia environmental pollution caused by Sb [4-6]. The Qingfeng and Xuanshan rivers, two main tributaries of the Zijiang River, have already been heavily polluted

*e-mail: haocm@ncist.edu.cn

by the discharge of mine water [7]. The Sb content in the river water varies from 0.02–8.12 mg/L, which is 36–1624 times higher than the maximum acceptable Sb concentration (0.005 mg/L) according to China's national drinking water quality standards [2, 3, 8]. It has been reported that the Sb concentration in the pollution source, the Sb mine drainage, has reached 6064–7502 µg/L [9]. In contrast, the Sb concentration in a non-polluted water body is below 1.0 µg/L [3, 10, 11]. With an increasing amount of attention paid to the surface water pollution, the source and the formation process of high Sb-containing mine water are often neglected. Hence, further investigation is of great importance to fully understand Sb sources and their geochemical behaviors.

In nature, Sb is mainly found as the sulfide mineral stibnite (Sb_2S_3). With the presence of oxygen, Sb can be mobilized into surrounding water bodies [11–13]. During this process, the chemical characteristic and isotope composition of the water bodies are changed. Hence, the formation process of Sb-contaminated water can be revealed by analyzing the chemical characteristics and isotope compositions of the surrounding water bodies. Sulfate is a useful marker for studying waters derived from both natural and anthropogenic sources. The elevated sulfate concentration in natural water is an indication of water deterioration [14]. Additionally, the sources, transportation, and transformation of the sulfate contaminants can be determined by analyzing the isotope compositions of sulfur and oxygen in sulfate anion [15–19]. Moreover, water-rock interactions have a strong influence on the chemical characteristics of water bodies [20–22]. For example, the dissolution of carbonate minerals leads to the rise of Ca^{2+} and Mg^{2+} contents, and the ion-exchange process often increases Na^+ and K^+ contents [22, 23].

The mining process of antimony deposits requires a high volume of drainage. When the amount of water inflow is greater than the amount of circulating water, the excess mine water must be discharged into the surrounding surface water body, resulting in Sb pollution. Hence, in this study, we investigated the source of Sb and geochemical behaviors of the mine drainage water using sulfate and oxygen isotope analysis and water-rock interaction method. The conclusions and observations obtained from this study provide valuable information for Sb pollutant source control and water body protection in the mine area.

Material and Methods

Study Area

This study was carried out in a 26 km² area in Xikuangshan Mine, which is in the northern part of Xiangzhong Basin. This mine is a monoclinical formation, which follows the axis of an anticline striking NE30° and plunging both at north and

south ends. The west wing has an F_{75} fracture and a boundary of a lamprophyre vein. The climate in this area is a monsoon-influenced humid subtropical climate with average precipitation and average evaporation of 1381.60 mm and 903.30 mm, respectively. Moreover, the average temperature of the Xikuangshan Mine is 16.70°C. Many gullies have been developed in the area, and the two main rivers are the Xuanshan and Qingfeng – seasonal rivers belonging to the Zijiang River system.

The antimony deposit is a layered breccia-type metal deposit in a structural fracture belt. The main mineral is stibnite. The aquifers, starting from top to bottom, are D_3x^4 (denoted as MA water) and D_3s^2 (denoted as SA water) [2, 24], which are dominated by fissure-karst water. They have poor water abundance and are mainly composed of mudstone, silicified limestone, and sandy limestone. Generally, the upper and lower aquifers have no hydraulic connection with each other.

The Sb mining history in Xikuangshan Mine dates to 1897 [25, 26]. After over 120 years of mining, a large amount of waste residues and ore pillars are abandoned in the goaf. It is estimated that the amount of Sb_2S_3 left in ore pillars is about 1.85 million tons. Due to the interaction between Sb minerals and oxygen gas, a significant amount of Sb element has been mobilized into the groundwater [26, 27].

Sample Collection and Analysis

A total of 25 water samples (including 11 mine water samples, 2 rainwater samples, 4 surface water samples, 4 MA water samples, and 4 SA water samples) were collected during the dry season between September and November in 2016 (Fig. 1). The surface water samples were collected from the Qingfeng River. Before collection, each sample bottle was washed with distilled water and followed with the water sample for 2–3 times. Each water sample was filtered by a 0.45 µm glass fiber membrane after collection and then filled three 500 mL sample bottles and one 10 L bottle. These three 500 mL samples were for hydrogen and oxygen isotope analysis, cation and anion concentration analysis, and Sb analysis, respectively. The 10 L sample was reserved for sulfur isotope analysis. Then, the pH values of the samples for Sb analysis and sulfur isotope analysis were adjusted to below 2.0 by adding 1:1 nitric acid (concentrated nitric acid/distilled water = 1/1). Lastly, a recovery indicator (an Sb solution) was added into each sample bottle followed with vigorous shaking.

The concentrations of major anions (chloride ions, bicarbonate ions, and sulfate ions) and major cations (calcium ions, magnesium ions, sodium ions, and potassium ions) in each water sample were determined by ion chromatography (Dionex Integration IC, Thermo Fisher, U.S.). The obtained data shows high analytical precision with low ionic balance error (generally within 5%). The Sb concentrations of the water samples were analyzed using an Agilent 7700 × inductively coupled

mass spectrometer (ICP-MS) with indium as the internal standard [2]. Each analysis was performed in triplicate to ensure precision and accuracy. The obtained data, which has less than 10% in the standard deviation and more than 95% recovery rate of the recovery indicator, was discussed in the following statistical analysis. The pH values and TDS values were obtained in the field by using a portable acidity meter (HANNA H18424) and an EC meter (HANNA H1833), respectively.

The analysis of stable isotope ^2H and $^{18}\text{O}(\text{H}_2\text{O})$ were performed by using a Micromass MultiPrep equipped with a dual inlet and an isotope ratio mass

spectrometers (IRMS) (Institute of Hydrogeology and Geology, Chinese Academy of Geological Sciences). The analytical uncertainties of the data obtained from this device are $\pm 0.1\%$ for $\delta^{18}\text{O}(\text{H}_2\text{O})$ and $\pm 1\%$ for $\delta^2\text{H}(\text{H}_2\text{O})$. The $\delta^{34}\text{S}(\text{SO}_4^{2-})$ and $\delta^{18}\text{O}(\text{SO}_4^{2-})$ values analysis were extracted as BaSO_4 with pH adjusted to less than 2 to prevent the formation of BaCO_3 . The $\delta^{34}\text{S}(\text{SO}_4^{2-})$ and $\delta^{18}\text{O}(\text{SO}_4^{2-})$ values were analyzed at the China University of Geosciences (Wuhan) using a Micromass IsoPrime stable IRMS. The analytical precision is 0.2‰.

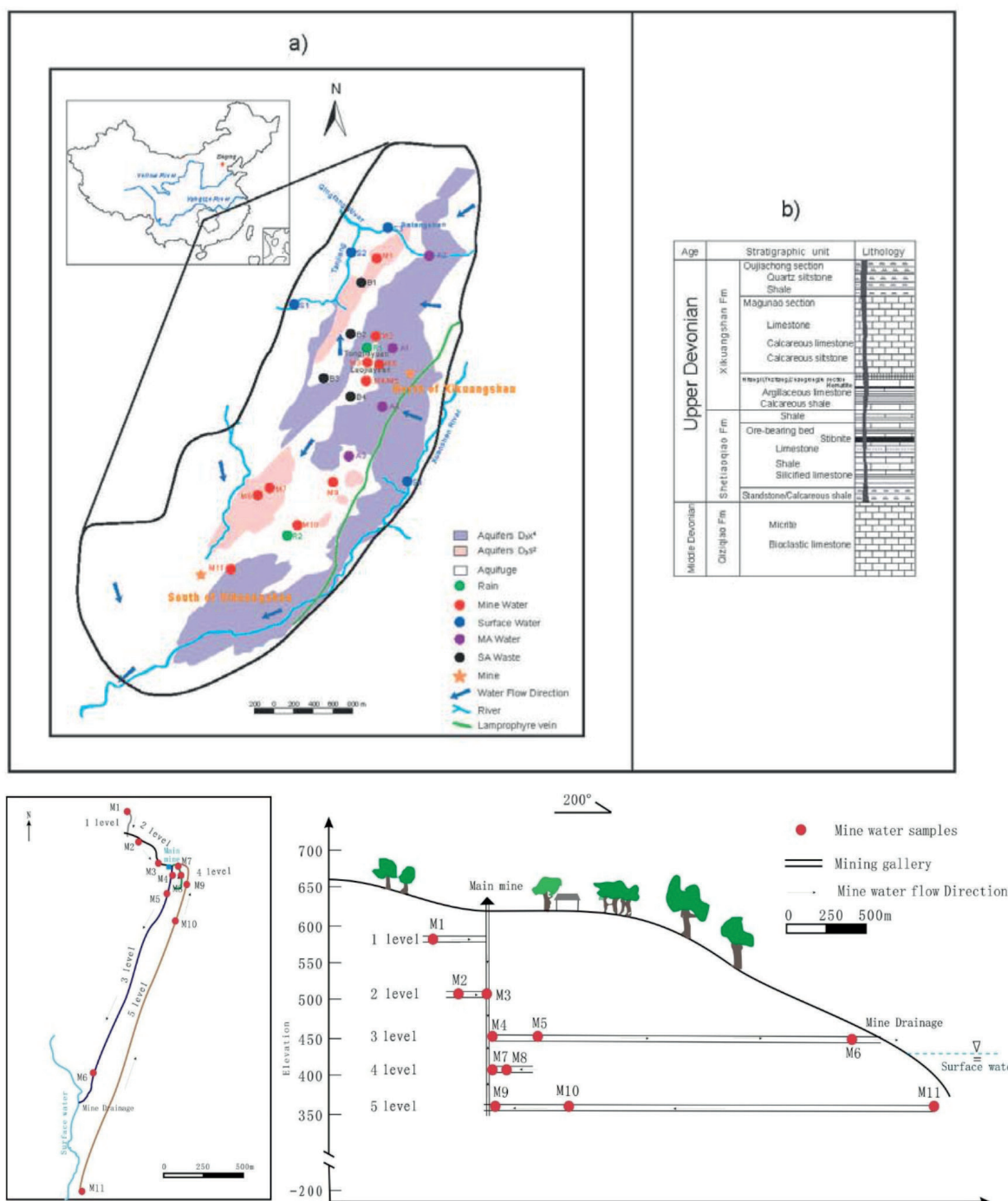


Fig. 1. Study area map and locations of sampling sites.

Results

Geochemical Characterization

The major ion concentration, Sb content, TDS content, pH, and isotope contents of each sample are listed in Table 1. The average Sb concentrations of mine water, rainwater, surface water, SA water, and MA water are 4.82 mg/L, 0.04 mg/L, 3.16 mg/L, 1.65 mg/L, and 0.21 mg/L, respectively – all of which exceed the maximum acceptable Sb concentration (0.005 mg/L) according to China’s national drinking water quality standards. The mine water sample, M6, has the highest Sb concentration among the collected water samples, which is 2420 times the maximum acceptable Sb concentration for drinking water, and 24.20 times of the maximum acceptable Sb concentration of wastewater (0.50 mg/L) according to the local discharge regulations (Hunan Province, China). Moreover, the Sb concentrations in different water bodies show a decreasing trend: mine water>surface water>SA water>MA water>rainwater. The relatively low Sb content in MA water and rainwater and the high Sb content in mine water indicates that the Sb pollution is caused by mining activities [2].

A Piper diagram is a graphical approach to represent the chemical characteristics and water-rock interactions of water samples [28]. The Piper diagram of these water samples was plotted in Fig. 2. According to the Piper classification, the hydrochemical types of mine water, rainwater, groundwater, SA water, and MA water are Ca-Na-SO₄ type, Ca-HCO₃ type, Ca-HCO₃-SO₄ type,

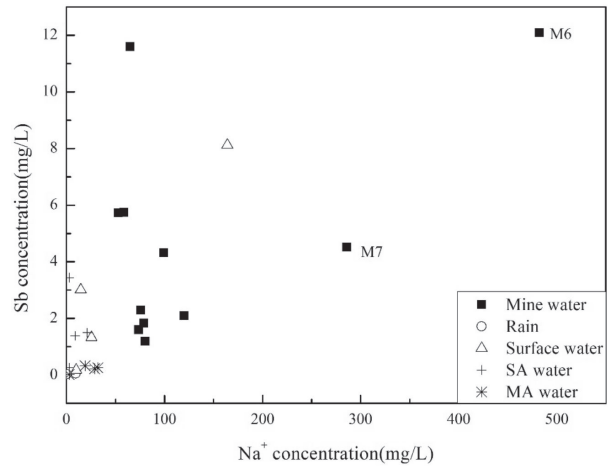


Fig. 3. Relationship between Na⁺ and Sb for samples collected in the study.

Ca-SO₄-HCO₃ type, and Ca-HCO₃-SO₄, respectively. Compared with other water bodies, the mine water has higher contents of Sb (Fig. 2), Na⁺ (Fig. 3), TDS (Fig. 4), and SO₄²⁻ (Fig. 5), suggesting that the Sb element is more likely to concentrate in high TDS, high Na⁺, and high SO₄²⁻ water bodies [2]. Moreover, the Sb contents in the mine water samples show a weak correlation with the contents of Na⁺, TDS, or SO₄²⁻ (Figs 2-5) – implying that the Sb in mine water originates from multiple sources.

The water-rock interaction process of Sb₂S₃ can be written as follows [15, 29]:

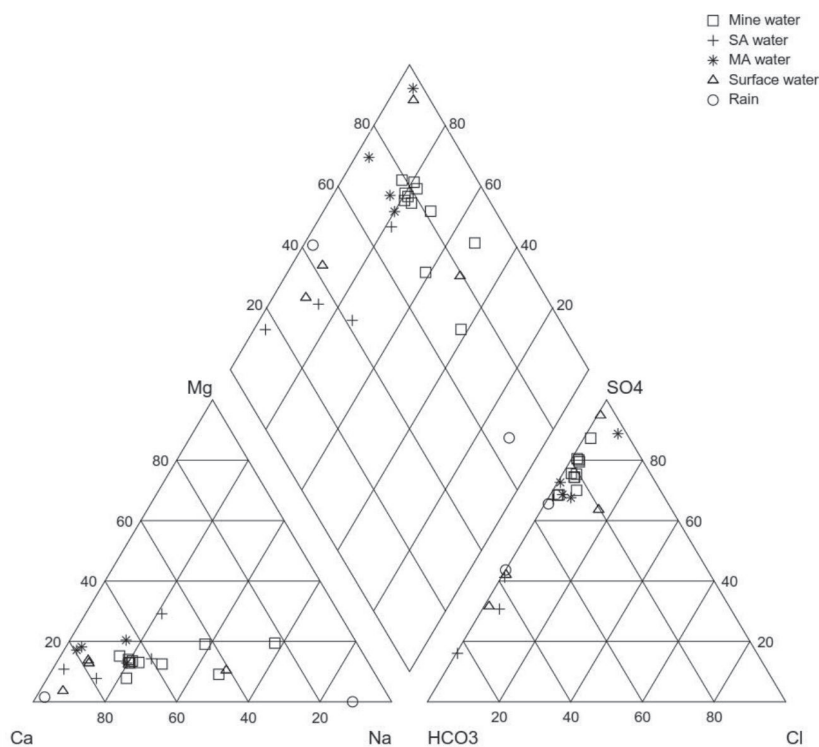


Fig. 2. Piper diagram of ionic composition of different groundwaters in the study area.

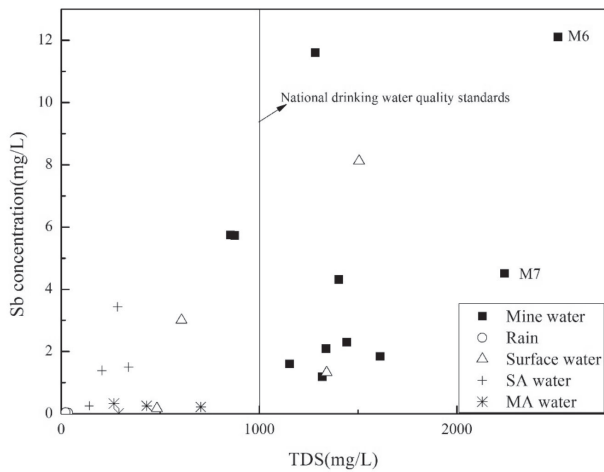


Fig. 4. Relationship between TDS and Sb for samples collected in the study; note: the TDS value of each sample was measured in the field using a portable EC meter (HANNA H1833).

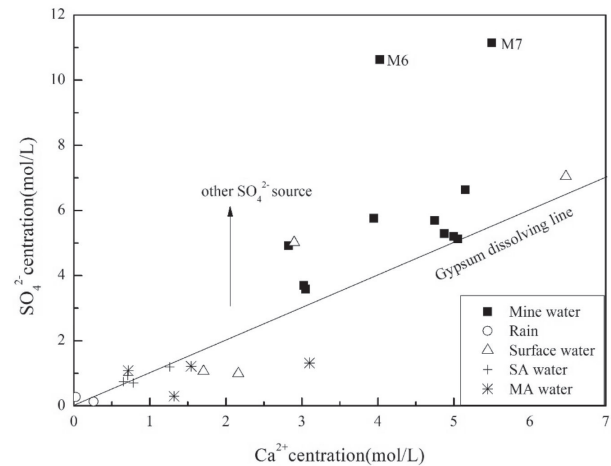


Fig. 6. Relationship between SO_4^{2-} and Ca^{2+} for samples collected in the study.

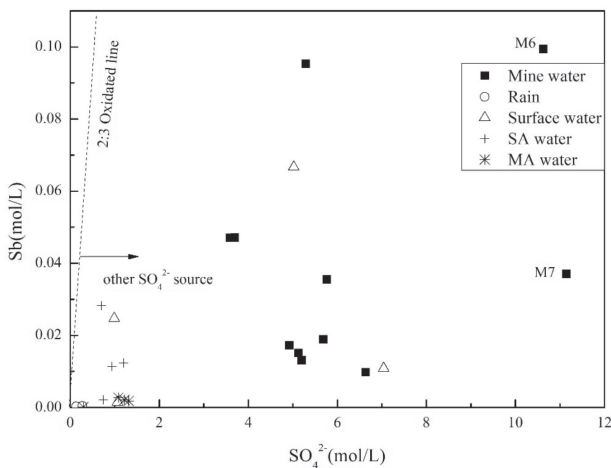
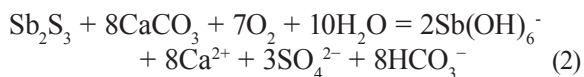


Fig. 5. Relationship between SO_4^{2-} and Sb for samples collected in the study.



As shown in Equation (1), a large amount of H^+ is produced. The pH values of mine water samples, however, range from 7.78 to 8.86, indicating that the H^+ produced from the water-rock interaction has been neutralized by carbonate mineral. If Sb_2S_3 is the only source of SO_4^{2-} in water bodies in this area, based on equation (2), the mole ratio between Sb element and SO_4^{2-} should be close to 2:3. However, as shown in Fig. 5, all collected water samples show a much higher concentration of SO_4^{2-} , indicating that the SO_4^{2-} in these water samples has multiple sources. Besides, as the solubility of $CaSO_4$ is much lower than that of $CaHCO_3$, with the rise of Ca^{2+} concentration, the content of SO_4^{2-} will decrease. As shown in Fig. 6, the actual

SO_4^{2-} contents of mine water samples are all above the gypsum dissolving line. This evidence further verifies the presence of other SO_4^{2-} sources.

Isotope Geochemistry

Analysis of 2H and ^{18}O Isotopes

Hydrogen and oxygen isotopic fractionation processes have been widely used in water source analysis and water cycle study. The isotope composition of water changes along with physicochemical processes, such as evaporation and water-rock interactions [30]. The $\delta^{18}O$ (H_2O) values and δ^2H values of these water samples were plotted in Fig. 7. Apart from M6 and M7 (labeled in Fig. 7), the $\delta^{18}O$ (H_2O) values and δ^2H values of mine water samples appear in-between the GMWL ($\delta^2H = 8\delta^{18}O(H_2O) + 10$) [31, 32] and LMWL ($\delta^2H = 8.38 \delta^{18}O(H_2O) + 17.3$) [33, 34], suggesting that these water samples are influenced by the evaporation effect. Besides, the high $\delta^{18}O$ (H_2O) values in M6 and M7 (labeled in Fig. 7) may be caused by the water-rock interaction [35].

The $\delta^{18}O(H_2O)$ and δ^2H values of SA water samples are very close to that of mine water samples (Fig. 7), indicating that SA water is the main water source of mine water. Moreover, one MA water sample, B4, and two surface water samples, S2 and S4 (highlighted in an outline of an ellipsoid in Fig. 7) show similar $\delta^{18}O(H_2O)$ and δ^2H values as mine water samples, suggesting that B4, S2, and S4 sampling sites have hydraulic connections with the mine water. As shown in Fig. 1, the discharged mine water may accumulate at S2 and S4 surface water sampling sites, which are located at the lowest position of all water bodies in this area. The evidence of the hydraulic connections between the MA water, B4, and mine water suggests that the mining activities have already destroyed the aquifuge between the SA aquifer and MA aquifer.

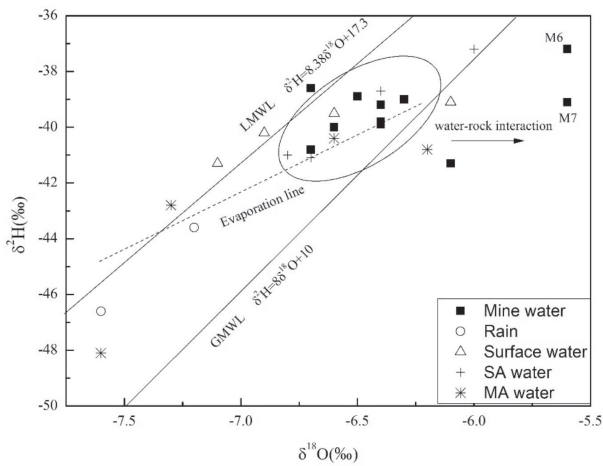


Fig. 7. Relationship between $\delta^{18}\text{O}$ (H_2O) and $\delta^2\text{H}$ for samples collected in the study.

Analysis of $^{34}\text{S}(\text{SO}_4^{2-})$ and $^{18}\text{O}(\text{SO}_4^{2-})$ Isotopes

$\delta^{34}\text{S}(\text{SO}_4^{2-})$ and $\delta^{18}\text{O}(\text{SO}_4^{2-})$ analysis plays an important role in studying the transformation and migration of the sulfur element in sulfide ore deposits [16, 18, 36]. In mine water samples, $\delta^{34}\text{S}(\text{SO}_4^{2-})$ ranges from -0.10‰ to $+6.10\text{‰}$ and $\delta^{18}\text{O}(\text{SO}_4^{2-})$ ranges from $+1.10\text{‰}$ to $+8.30\text{‰}$. Multiple sulfate minerals found in this mine, including pyrite (-0.78‰ to $+33.40\text{‰}$), lamprophyre (-6.30‰ to $+2.30\text{‰}$), stibnite (-3.27‰ to $+16.83\text{‰}$), and gypsum (-3.27‰ to $+16.83\text{‰}$), contribute to the sulfate cations in the mine water samples [37, 38]. The $\delta^{34}\text{S}(\text{SO}_4^{2-})$ values of mine water samples agree well with the $\delta^{34}\text{S}(\text{SO}_4^{2-})$ values of these sulfate minerals (Fig. 8).

Discussion

Water-Rock Interaction

The $\text{Ca}^{2+}/\text{Na}^+$ and $\text{Mg}^{2+}/\text{Na}^+$ mole ratios in a water body is closely related to the dissolution process of evaporites, carbonates, and silicates during the water-rock interaction [23]. As shown in Fig. 9, the mole ratios of $\text{Ca}^{2+}/\text{Na}^+$ and $\text{Mg}^{2+}/\text{Na}^+$ of all these water samples appear between carbonate and silicate dissolution, indicating that the chemical composition of water bodies in this area is influenced by carbonates and silicates. Compared with SA water, the $\text{Ca}^{2+}/\text{Na}^+$ and $\text{Mg}^{2+}/\text{Na}^+$ mole ratios of mine water samples, especially M6 and M7, are closer to the silicate dissolution, suggesting that the mine water contains a high level of silicate minerals (Table 1).

The relationship between cations and anions in a water body is a powerful indicator of the source and evolution process of its chemical composition. For instance, the influence of ion-exchange interaction on the chemical composition of a water body can be evaluated by the concentration of $(\text{Ca}^{2+} + \text{Mg}^{2+} - \text{HCO}_3^- - \text{SO}_4^{2-})$ versus the concentration of $(\text{Na}^+ + \text{K}^+ - \text{Cl}^-)$ in meq/L [39-42]. With a strong ion-exchange interaction, the data points of water samples will lie along a line with a slope of -1 . The concentration of $(\text{Ca}^{2+} + \text{Mg}^{2+} - \text{HCO}_3^- - \text{SO}_4^{2-})$ versus the concentration of $(\text{Na}^+ + \text{K}^+ - \text{Cl}^-)$ in meq/L was plotted in Fig. 9 [43]. All the data points of the mine water samples are in the second quadrant of the plot, indicate an access amount of Na and K cations, which is evidence of ion-exchange reactions during the water-rock interaction of mine water. Additionally, the data points of these mine water samples (except M7 and M6) follow the fitting line with a slope of -1 , suggesting

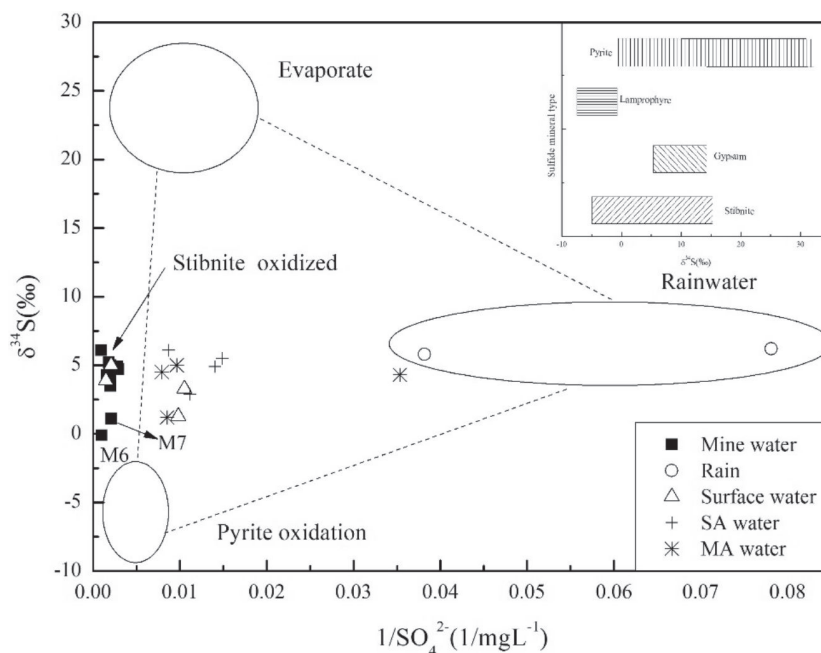


Fig. 8. Relationship between $\delta^{34}\text{S}$ (SO_4^{2-}) and inverse of SO_4^{2-} for samples collected in the study.

Table 1. Geochemical data for samples collected in the study; values less than 0.01mg/L LOD (limit of detection) were set to zero for statistical purposes.

Samples	K ⁺	Na ⁺	Ca ²⁺	Mg ²⁺	SO ₄ ²⁻	Cl ⁻	HCO ₃ ⁻	Sb	TDS	pH	‰			
											δ ² H	δ ¹⁸ O(H ₂ O)	δ ³⁴ S(SO ₄ ²⁻)	δ ¹⁸ O(SO ₄ ²⁻)
M1	7.20	71.80	202.00	23.60	492.00	34.30	208.40	1.84	1612.00	7.89	-38.60	-6.30	5.00	1.10
M2	11.00	54.10	195.00	26.20	508.00	19.50	177.20	11.60	1283.00	8.21	-40.80	-6.70	4.00	1.80
M3	8.50	49.80	121.00	14.90	355.00	13.10	132.50	5.74	855.00	8.08	-39.20	-6.40	4.90	3.00
M4	6.90	68.80	190.00	12.80	546.00	7.80	154.80	2.30	1443.00	7.86	-41.30	-6.10	5.20	8.30
M5	8.40	44.60	122.00	15.20	344.00	13.40	128.00	5.73	876.00	8.06	-38.90	-6.50	4.70	3.00
M6	16.00	466.00	161.00	82.90	1020.00	27.70	547.90	12.10	2510.00	8.86	-37.20	-5.60	-0.10	1.80
M7	12.80	273.00	220.00	27.70	1070.00	17.50	168.20	4.51	2240.00	8.21	-39.10	-5.60	6.10	4.60
M8	8.70	71.60	206.00	24.30	637.00	13.00	178.70	1.19	1319.00	7.95	-39.80	-6.40	4.30	1.50
M9	6.20	93.00	158.00	20.70	553.00	13.80	157.80	4.32	1403.00	7.84	-39.00	-6.30	4.20	2.70
M10	2.90	117.00	113.00	30.70	472.00	11.20	257.60	2.10	1338.00	7.78	-39.90	-6.40	1.10	3.70
M11	5.80	67.60	200.00	25.60	499.00	11.60	184.60	1.60	1153.00	8.33	-40.00	-6.60	3.50	2.50
R1	0.00	0.30	10.40	0.10	12.80	0.00	21.00	0.03	35.00	7.12	-46.60	-7.60	6.20	11.30
R2	0.20	9.40	1.00	0.00	26.20	0.30	17.00	0.05	22.00	6.87	-43.60	-7.20	5.80	10.40
S1	1.40	8.50	68.20	7.30	102.00	1.60	175.70	0.18	483.00	8.18	-40.20	-6.90	1.30	3.00
S2	3.00	11.60	86.50	8.60	95.10	3.10	256.10	3.01	607.00	7.76	-39.50	-6.60	3.30	4.10
S3	4.10	21.40	259.00	6.30	676.00	4.50	38.70	1.33	1341.00	10.79	-41.30	-7.10	3.90	-1.90
S4	6.10	158.00	116.00	17.90	482.00	89.30	196.50	8.12	1505.00	8.57	-39.10	-6.10	5.00	5.80
B1	4.30	16.80	50.40	5.80	115.00	4.20	59.60	1.5	340.00	7.87	-38.70	-6.40	6.10	3.20
B2	1.10	1.60	31.30	4.10	67.30	4.60	33.10	3.44	284.00	8.26	-41.10	-6.70	5.50	4.20
B3	0.90	8.00	28.40	5.50	89.70	0.70	41.70	1.39	205.00	6.43	-41.00	-6.80	2.90	1.40
B4	1.10	1.70	26.00	3.70	71.30	5.20	2.50	0.26	141.00	8.01	-37.20	-6.00	4.90	3.00
A1	0.60	2.20	52.70	4.00	28.30	0.50	187.60	0.02	290.00	7.88	-42.80	-7.30	4.30	5.10
A2	1.60	30.60	61.80	8.90	117.00	2.00	208.40	0.26	432.00	8.02	-40.80	-6.20	1.20	2.40
A3	5.10	14.10	28.60	10.20	104.00	1.80	61.90	0.33	266.00	8.63	-48.10	-7.60	5.00	4.70
A4	4.00	24.90	124.00	7.40	126.00	14.30	336.50	0.22	705.00	7.54	-40.40	-6.60	4.50	5.50

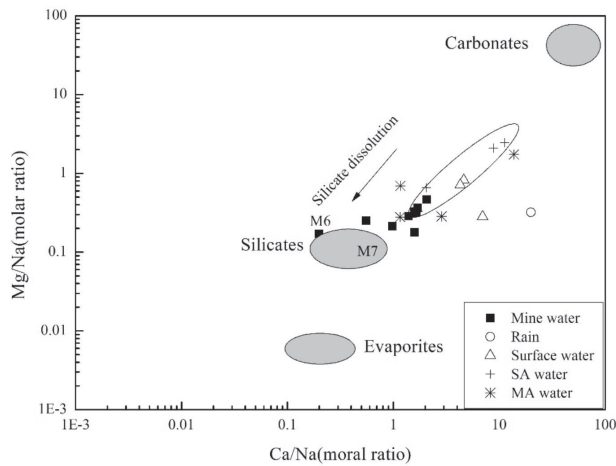


Fig. 9. Diagrams for determining the end member compositions by Mg/Na vs. Ca/Na molar ratios.

that the ion-exchange process plays a key role in the formation of mine water. Besides, M7 and M6 appear above the fitting line with higher concentrations of Ca cation and Mg cation compared with that of other mine water samples. As M6 and M7 are collected at the main drainage of the mine water (Fig. 10), the high flow rate promotes the dissolution of carbonate minerals. Moreover, compared with the SA water samples, the mine water samples have high (Na⁺+K⁺-Cl⁻), which is additional evidence of cation ion-exchange interaction that occurred during the formation of the mine water.

The Source of SO₄²⁻ in Mine Water

The relationship between δ³⁴S(SO₄²⁻) and the inverse value of SO₄²⁻ content is commonly used to analyze the source of sulfate in a water body [18, 19, 44]. The δ³⁴S(SO₄²⁻) and the 1/SO₄²⁻ of the samples, as well as the value ranges of δ³⁴S(SO₄²⁻) and 1/SO₄²⁻ of three

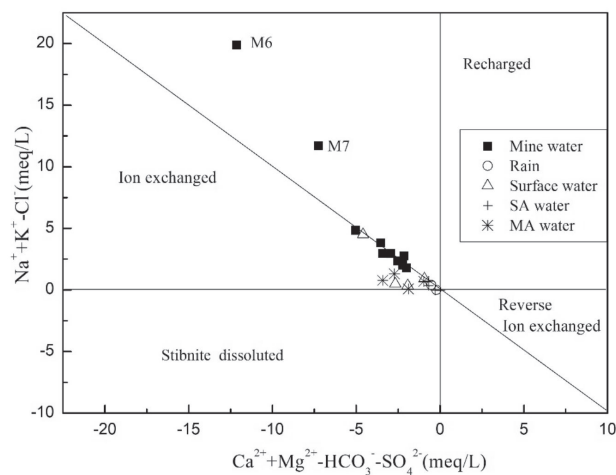


Fig. 10. Relationship between Ca²⁺+ Mg²⁺-HCO₃⁻-SO₄²⁻ and Na⁺+K⁺-Cl⁻ for samples collected in the study.

main sulfate sources (sulfide oxidation, evaporate, and rainwater) were plotted in Fig. 8. The sulfide oxidation appears in the bottom left side of the plot with a high SO₄²⁻ concentration and low δ³⁴S(SO₄²⁻), because of the influence of a sulfate-reducing bacteria [15, 19, 26]. The evaporated sulfate source with high SO₄²⁻ and high δ³⁴S(SO₄²⁻) appears in the upper left of the plot. The rainwater generally has a low level of SO₄²⁻ and a medium level of δ³⁴S(SO₄²⁻) and lies in the middle right of the plot (Fig. 8).

Generally, the smaller the distance between a sulfate source and a water sample in the plot, the stronger the influence of the sulfate source on the sulfate in a water sample becomes, and *vice versa*. As shown in Fig. 7, the data points of the mine water samples lie close to the sulfide oxide source, suggesting that sulfide oxidation is the main source of the sulfate cations in mine water. Rainwater is not the source of the sulfate cations in mine water due to the large differences in sulfate concentrations. This statement can also be confirmed in the δ¹⁸O(H₂O) and the δ²H analysis in Fig. 7. Compared with the SA water, the mine water has a higher concentration of SO₄²⁻.

The relative proportions of oxygens derived from water can be calculated by the following equation [44-46]:

$$\delta^{18}\text{O}(\text{SO}_4^{2-}) = X (\delta^{18}\text{O}(\text{H}_2\text{O}) + \text{EH}_2\text{O}) + (1-X) (\delta^{18}\text{O}(\text{O}_2) + \text{EO}_2) \quad (3)$$

...where X is a coefficient and EH₂O and EO₂ are the isotope enrichment factors for the incorporation of oxygen from water and atmospheric oxygen, respectively. Fig. 11 was plotted based on the data calculated from Equation (3).

As shown in Fig. 11, about 75% percent of sulfate oxygen atoms in the mine water (except the M4 sample) is derived from water. This result agrees with previous works, where Sun et al. and Seal et al. investigated

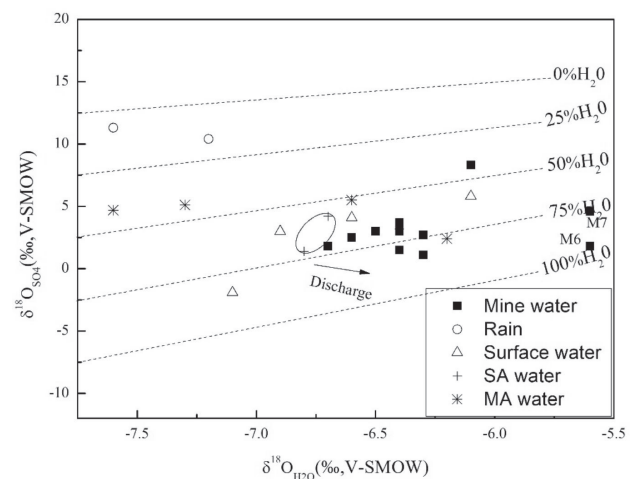
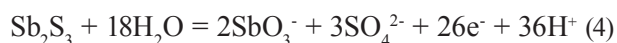


Fig. 11. Diagram comparing the δ¹⁸O composition of aqueous SO₄ and coexisting water for samples collected in the study.

the source of oxygen atoms in sulfate cations produced from the oxidation reaction between sulfide ore (brilliant and pyrite) and excess oxygen [44, 47]. As the sulfur element of the sulfite cations in the mine water comes from the sulfide oxidation process, the formation of high Sb water can be described as follows [9, 13]:



In this process, oxygen atoms in $\text{Sb}(\text{OH})_6^-$ are mainly derived from the oxygen gas. Oxidation of sulfide to sulfate, however, does not occur on the same timescale as the mobilization of antimony. Sulfate is possibly the final product of a sequence of slow reactions, in which algae and bacteria take the sulfur from its initial oxidation state -2 to +6 [13, 29, 48, 49]. Additionally, oxygen atoms in SO_4^{2-} in M6 and M7 are mostly derived from water, which may also be due to the high water-flow rate in their sampling site.

Formation Process of High Sb Mine Water

Given the evidence presented above for the antimony source of the mine water, the question is: how did this phenomenon occur?

It has been confirmed that the source of the antimony of the mine water comes from the oxidation of Sb_2S_3 . The formation process of the high Sb mine water is described as follows. The MA water and the SA water generally have low Sb concentration (<0.6 mg/L) and the Sb element is mainly present in stibnite ore, which is a reducing environment. Once the ore body is exposed, the closed reducing environment immediately becomes an oxidizing environment. With the presence of an excess amount of oxygen gas, the sulfite in stibnite ore is oxidized to S^{4+} or S^{6+} (Equation (4)) and the Sb is oxidized to SbO_3^- , a water-soluble anion (Equation (5)). This process also produces a large amount of H^+ as a by-product, which is rapidly neutralized by carbonate ores presented in the mine. Before the depletion of carbonate ores, the mine water will not become acidic, and the oxidation of stibnite will continue, resulting in high Sb mine water [49-51].

For safety reasons, the mining process requires continuous drainage, during which a large amount of drainage continuously flows into the groundwater funnel area or the lowest discharge area. Moreover, the accumulation of a large amount of mine water accelerates the formation of $\text{Sb}(\text{OH})_6^-$ (Equations 4-6). Besides, when the mine water flows to the groundwater funnel area or the lowest discharge zone, part of

the Ca^{2+} in the mine water is replaced by Na^+ and K^+ in surrounding rock (silicified limestone) through ion-exchange interactions, resulting in a reduction of Ca^{2+} concentration and a rise of Na^+ and K^+ concentrations. The high Na^+ and high K^+ water further contribute to the rise of the Sb content in the mine water. Thus, mine water with high Sb, high sulfate salt, and high TDS is formed.

Conclusions

The mining process of the antimony deposit requires a large amount of drainage. As the amount of water inflow is greater than the amount of circulating water, the excess mine water must be discharged into the surrounding surface water bodies, resulting in Sb pollution. Recently, the surface water pollution from discharged mine water has received widespread attention. The sources and the formation processes of high Sb mine water are often neglected. In this study, the $\delta^{34}\text{S}(\text{SO}_4)$ and $\delta^{18}\text{O}(\text{H}_2\text{O})$ data and the water-rock interactions are analyzed to reveal the Sb sources and geochemical behaviors of the mine drainage water in the largest Sb mine in China. The main conclusions obtained from this research are listed as follows:

1) The Sb concentrations in the mine water samples range from 1.19 mg/L to 12.10 mg/L with an average of 4.82 mg/L, which is 238-2420 times of China's national drinking water quality standards (0.005 mg/L) and 24.20 times the maximum acceptable Sb concentration of wastewater (0.50 mg/L), according to the local discharge regulations (Hunan Province, China). The chemical composition of the mine water is Ca-Na- SO_4 type. The TDS value ranges from 855.00 to 2510.00 mg/L, with an average of 1457.45 mg/L, owing to the intensive mining activities.

2) The Sb contents in different water bodies vary a lot and have the following trend: mine water > groundwater > SA water > MA water > rain. Compared with other water bodies, the mine water has a higher amount of Na^+ , TDS, and SO_4^{2-} , indicating that the Sb element is more easily accumulated in the water bodies with high Na^+ , high TDS, and High SO_4^{2-} .

3) The $\delta^{18}\text{O}(\text{H}_2\text{O})$ and $\delta^2\text{H}$ in the mine water samples are consistent with that of the SA water, indicating that the SA water is the main source of the mine water. Part of the MA water samples show a similar level of $\delta^{18}\text{O}(\text{H}_2\text{O})$ and $\delta^2\text{H}$, suggesting that the MA aquifers are another water source of the mine water.

4) The Sb in the mine water is mainly derived from the oxidation of stibnite. The surplus carbonate minerals accelerate the oxidation reaction of Sb_2S_3 , resulting in high Sb content mine water. Moreover, soluble oxygen in mine water promotes the formation of soluble $\text{Sb}(\text{OH})_6^-$. The high content of Na^+ and K^+ induced by the ion-exchange interaction also leads to the rise of Sb content in the mine water.

Acknowledgements

The authors gratefully acknowledge the financial support provided by the Open Fund of State Key Laboratory of Groundwater Protection and Utilization by Coal Mining (No. SHJT-17-42.17), the Langfang Technology Research and Development Program (2018011064), the Fundamental Research Funds for the Central Universities of China (3142018009), and the Key Laboratory of Mine Geological Hazards Mechanism and Control Project (KF2017-13).

Conflict of Interest

The authors declare no conflict of interest.

References

- HE M.C., WANG N.N., LONG X.J., ZHANG C.J., MA C.L., ZHONG Q.Y., WANG A.H., WANG Y., PERVAIZ A., SHAN J. Antimony speciation in the environment: Recent advances in understanding the biogeochemical processes and ecological effects. *J Environ Sci (China)*, **75**, 14, **2019**.
- FU Z.Y., WU F.C., AMARASIRIWARDENA D., MO C.L., LIU B.J., ZHU J., DENG Q.J., LIAO H.Q. Antimony, arsenic and mercury in the aquatic environment and fish in a large antimony mining area in Hunan, China. *Sci Total Environ*, **408** (16), 3403, **2010**.
- WEN B., ZHOU J.W., ZHOU A.G., XIE L.N. Sources, migration and transformation of antimony contamination in the water environment of Xikuangshan, China: Evidence from geochemical and stable isotope (S, Sr) signatures. *Sci Total Environ*, **569-570**, 114, **2016**.
- WANG N.N., WANG A.H., KONG L.H., HE M.C. Calculation and application of Sb toxicity coefficient for potential ecological risk assessment. *Sci Total Environ*, **610-611**, 167, **2018**.
- WANG N.N., WANG A.H., XIE J., HE M.C. Responses of soil fungal and archaeal communities to environmental factors in an ongoing antimony mine area. *Sci Total Environ*, **652**, 1030, **2019**.
- HU X.Y., HE M.C., LI S.S., GUO X.J. The leaching characteristics and changes in the leached layer of antimony-bearing ores from China. *Journal of Geochemical Exploration*, **176**, 76, **2017**.
- XU D.Y., GAO B., PENG W.Q., LI Y.Y. Geochemical and health risk assessments of antimony (Sb) in sediments of the Three Gorges Reservoir in China. *Science of The Total Environment*, **660**, 1433, **2019**.
- WANG X.Q., HE M.C., XI J.H., LU X.F. Antimony distribution and mobility in rivers around the world's largest antimony mine of Xikuangshan, Hunan Province, China. *Microchemical Journal*, **97** (1), 4, **2011**.
- ZHU J. Environmental characteristics of water near the Xikuangshan antimony mine, Hunan Province. *Acta Scientiae Circumstantiae*, **29** (2), 655, **2009**.
- FILELLA M.B.N., CHEN J. Antimony in the environment a review focused on natural waters II. Relevant solution chemistry. *Earth Science Reviews*, **59**, 265, **2002**.
- ZHU J., GUO J. Overview on Research on Environmentally Geochemical Characteristics of Antimony. *Earth and Environment*, **38** (1), 109, **2010**.
- HERATH I., VITHANAGE M., BUNDSCHUH J. Antimony as a global dilemma: Geochemistry, mobility, fate and transport. *Environ Pollut*, **223**, 545, **2017**.
- ASHLEY P.M., CRAW D., GRAHAM B.P., CHAPPELL D.A. Environmental mobility of antimony around mesothermal stibnite deposits, New South Wales, Australia and southern New Zealand. *Journal of Geochemical Exploration*, **77** (1), 1, **2003**.
- BOTTRELL S., TELLAM J., BARTLETT R., HUGHES A. Isotopic composition of sulfate as a tracer of natural and anthropogenic influences on groundwater geochemistry in an urban sandstone aquifer, Birmingham, UK. *Applied Geochemistry*, **23** (8), 2382, **2008**.
- NARIYAN E., WOLKERSDORFER C., SILLANPAA M. Sulfate removal from acid mine water from the deepest active European mine by precipitation and various electrocoagulation configurations. *J Environ Manage*, **227**, 162, **2018**.
- SAMBORSKA K., HALAS S. ³⁴S and ¹⁸O in dissolved sulfate as tracers of hydrogeochemical evolution of the Triassic carbonate aquifer exposed to intense groundwater exploitation (Olkusz-Zawiercie region, southern Poland). *Applied Geochemistry*, **25** (9), 1397, **2010**.
- TEMOVSKI M., FUTO I., TURI M., PALCSU L. Sulfur and oxygen isotopes in the gypsum deposits of the Provalata sulfuric acid cave (Macedonia). *Geomorphology*, **315**, 80, **2018**.
- ZHOU J.W., ZHANG Q.X., KANG F.X., ZHANG Y.P., YUAN L., WEI D., LIN S.H. Using multi-isotopes (³⁴S, ¹⁸O, ²H) to track local contamination of the groundwater from Hongshan-Zhaili abandoned coal mine, Zibo city, Shandong province. *International Biodeterioration & Biodegradation*, **128**, 48, **2018**.
- GAMMONS C.H., BROWN A., POULSON S.R., HENDERSON T.H. Using stable isotopes (S, O) of sulfate to track local contamination of the Madison karst aquifer, Montana, from abandoned coal mine drainage. *Applied Geochemistry*, **31**, 228, **2013**.
- LI Q.G., JU Y.W., LU W.Q., WANG G.C., NEUPANE B., SUN Y. Water-rock interaction and methanogenesis in formation water in the southeast Huaibei coalfield, China. *Marine and Petroleum Geology*, **77**, 435, **2016**.
- REDWAN M., ABDEL MONEIM A.A., AMRA M.A. Effect of water-rock interaction processes on the hydrogeochemistry of groundwater west of Sohag area, Egypt. *Arabian Journal of Geosciences*, **9** (2), **2016**.
- SALCEDO SANCHEZ E.R., GARRIDO HOYOS S.E., VICENTA ESTELLER M., MORALES M.M., ASTUDILLO A.O. Hydrogeochemistry and water-rock interactions in the urban area of Puebla Valley aquifer (Mexico). *Journal of Geochemical Exploration*, **181**, 219, **2017**.
- TALAVERA MENDOZA O., RUIZ J., DIAZ VILLASENOR E., RAMIREZ GUZMAN A., CORTES A., SALGADO SOUTO S.A., DOTOR ALMAZAN A., RIVERA BUSTOS R. Water-rock-tailings interactions and sources of sulfur and metals in the subtropical mining region of Taxco, Guerrero (southern Mexico): A multi-isotopic approach. *Applied Geochemistry*, **66**, 73, **2016**.
- ZHOU J.W., NYIRENDA M.T., XIE L.N., ZHOU B.L., ZHU Y., LIU H.L. Mine waste acidic potential and distribution of antimony and arsenic in waters of the

- Xikuangshan mine, China. *Applied Geochemistry*, **77**, 52, **2017**.
25. FU Z.Y., WU F.C., MO C.L., DENG Q.J., MENG W., GIESY J.P. Comparison of arsenic and antimony biogeochemical behavior in water, soil and tailings from Xikuangshan, China. *Sci Total Environ*, **539**, 97, **2016**.
 26. WEN B., ZHOU A.G., ZHOU J.W., LIU C.F., HUANG Y.L., LI L.G. Coupled S and Sr isotope evidences for elevated arsenic concentrations in groundwater from the world's largest antimony mine, Central China. *Journal of Hydrology*, **557**, 211, **2018**.
 27. GUO X.J., WU Z.J., HE M.C., MENG X.G., JIN X., QIU N., ZHANG J. Antimony smelting process generating solid wastes and dust: characterization and leaching behaviors. *J Environ Sci (China)*, **26** (7), 1549, **2014**.
 28. PIPER M. Graphic procedure in the geochemical interpretation of water-analyses. *Hydrology*, 914, **1944**.
 29. BIVER M., SHOTYK W. Stibnite (Sb₂S₃) oxidative dissolution kinetics from pH 1 to 11. *Geochimica et Cosmochimica Acta*, **79**, 127, **2012**.
 30. TAHERI M., MAHMUDY GHARAIE M.H., MEHRZAD J., AFSHARI R., DATTA S. Hydrogeochemical and isotopic evaluation of arsenic contaminated waters in an argillic alteration zone. *Journal of Geochemical Exploration*, **175**, 1, **2017**.
 31. GAMMONS C.H., POULSON S.R., PELLICORI D.A., REED P.J., ROESLER A.J., PETRESCU E.M. The hydrogen and oxygen isotopic composition of precipitation, evaporated mine water, and river water in Montana, USA. *Journal of Hydrology*, **328** (1-2), 319, **2006**.
 32. CRAIG H. Isotopic Variations in Meteoric Waters. *SCIENCE*, **133**, 1702, **1961**.
 33. WU H., ZHANG X., SUN G. Variations of stable Isotope Characteristics of Atmospheric Precipitation from Changsha, Hunan. *Resources and Environment in the Yangtze Basin*, **21** (5), 540, **2012**.
 34. HUANG Y., ZHANG X., TANG F. Variations of Precipitation Stable Isotope and Vapor Origins Revealed by Deuterium Excess in Changsha. *JOURNAL OF NATURAL RESOURCE*, **28** (11), 1945, **2013**.
 35. HAO C.M., HUANG Y., MA D.J. Isotope Drift Characteristics in Ordovician Limestone Karst Water Caused by Coal Mining in Northern China. *Mine Water and the Environment*, **2019**.
 36. KIM D.M., YUN S.T., YOON S.M., MAYER B. Signature of oxygen and sulfur isotopes of sulfate in ground and surface water reflecting enhanced sulfide oxidation in mine areas. *Applied Geochemistry*, **100**, 143, **2019**.
 37. YANG S. On Inquiry about the Genesis of Human Stibnite ore and the direction of the Search. *Hunan Geology*, **5** (4), 12, **1986**.
 38. TAO Y., GAO Z., JIN J. The Origin of Ore Forming Fluid of Xikuangshan Type Antimony Deposits in Central Hunan Province. *Geology Geochemistry*, **29** (1), 14, **2001**.
 39. LIU J., CAI W., CAO Y. Hydrochemical Characteristics of Groundwater and the origin in Alluvial-proluvial Fan of Qinhe River. *Environmental Science*, **39** (12), 5428, **2018**.
 40. JALALI M. Major ion chemistry of groundwaters in the Bahar area, Hamadan, western Iran. *Environmental Geology*, **47** (6), 763, **2005**.
 41. KIM K.J., RAJMOHAN N., KIM H.J., HWANG G.S., CHO M.J. Assessment of groundwater chemistry in a coastal region (Kunsan, Korea) having complex contaminant sources: a stoichiometric approach. *Environmental Geology*, **46** (6-7), 7634, **2004**.
 42. GUO H., WANG Y. Geochemical characteristics of shallow groundwater in Datong basin, northwestern China. *Journal of Geochemical Exploration*, **87** (3), 109, **2005**.
 43. KAUR L., RISHI M.S., SHARMA S., SHARMA B., LATA R., SINGH G. Hydrogeochemical characterization of groundwater in alluvial plains of river Yamuna in northern India: An insight of controlling processes. *Journal of King Saud University - Science*, **2019**.
 44. SUN J., KOBAYASHI T., STROSNIDER W.H.J., WU P. Stable sulfur and oxygen isotopes as geochemical tracers of sulfate in karst waters. *Journal of Hydrology*, **551**, 245, **2017**.
 45. TAYLOR B.E., WHEELER M.C. Sulfur- and Oxygen-Isotope Geochemistry of Acid Mine Drainage in the Western United States. **550**, 481, **1993**.
 46. SUN J., TANG C.Y., WU P., STROSNIDER W.H.J., HAN Z.W. Hydrogeochemical characteristics of streams with and without acid mine drainage impacts: A paired catchment study in karst geology, SW China. *Journal of Hydrology*, **504**, 115, **2013**.
 47. SEAL S., KUIRY S.C., HEINMEN B. Effect of glycine and hydrogen peroxide on chemical-mechanical planarization of copper. *Thin Solid Films*, **423**, 243, **2003**.
 48. LI S.X., ZHENG F.Y., HONG H.S. Photo-oxidation of Sb(III) in the seawater by marine phytoplankton-transition metals-light system. *Chemosphere*, **65** (8), 1432, **2006**.
 49. WANG X.Q., HE M.C., LIN C.Y., GAO Y.X., ZHENG L. Antimony(III) oxidation and antimony(V) adsorption reactions on synthetic manganite. *Geochemistry*, **72**, 41, **2012**.
 50. GUO X., WU Z., HE M. Removal of antimony(V) and antimony(III) from drinking water by coagulation-flocculation-sedimentation (CFS). *Water Res*, **43** (17), 4327, **2009**.
 51. XI J., HE M., LIN C. Adsorption of antimony(III) and antimony(V) on bentonite: Kinetics, thermodynamics and anion competition. *Microchemical Journal*, **97** (1), 85, **2011**.